12

Sensorless Control of a Polar-Axis Photovoltaic Tracking System

John T. Agee and Adisa A. Jimoh
Tshwane University of Technology
P. Bag X680 Pretoria 0001,
South Africa

1. Introduction

Photovoltaic solar power installations can be broadly classified as static (non-tracking), single-axis tracking, polar axis-tracking and two-axis tracking installations (Agee et al., 2006). In general, tracking photovoltaic systems have higher percentage energy recovery per Kilowatt of installed capacity than static solar power systems (Ed. Kusoke et al., 2003). A key component of existing photovoltaic tracking systems is the solar position sensor and associated conditioning circuitry, which provides the information with which the tracking angle is updated. These sensors add to the overall cost of installed photovoltaics. For example, in South Africa where the average installed cost of photovoltaics is ZAR 29.00/Watt (Greenology, 2010), the percentage sensor(s) cost for installed photovoltaic wattage is shown in Figure 1, based on an average sensor cost of USD110.0. It is evident from Figure 1 that for low power solar photovoltaic applications, the percentage sensor cost motivates the exploitation of alternative tracking strategies that are devoid of sensors. Sensor-less tracking offer a cost effective solution in such low power applications. Sensor-less tracking has been reported in literature (Ibrahim et al., 2004; Cheng & Wong, 2009; Power from the Sun, 2010; Chen et al., 2006; Stine & Harrington, 1988) concerning solar-thermal systems. These rely on the use of well established astronomical formulae to extract the direction of sunrays as a function of the local clock time, after due compensation for any differences between the local clock time and the solar time. The equation of time (EOT) and the local longitude compensation are factored into the derivation of the final local time equation. EOT is an equation that evaluates the difference between the local clock time and the solar hour. In the discourse presented in the current chapter, the sensor-less tracking of a polar-axis solar tracker is reported. The concepts of differential flatness (Fliess et al.; Fliesss et al.; Levine & Nguyen, 2003; Bitaud, 1990, 1997, 2003) is used for embedding the equations of the direction of sunrays into the feedback loop of the controller.

In the rest of the chapter, the physical structure of the polar-axis solar tracker and the derivation of its dynamic equations are described in section two. The concepts of differential flatness and the derivation of the flat output for the polar-axis solar tracker is presented in section three. Controller design is contained in section four. A derivation of the relationship between the local clock time and the direction of sunrays with respect to an observer (or the photovoltaics platform) at a given location, together with the integration of time-based values of the sunrays angle for sensor-less tracking is presented in section five of the

chapter. Illustrative simulations and results presentation and discussion form section six of the chapter. Conclusions are presented in section seven. A list of references is included at the end of the chapter.

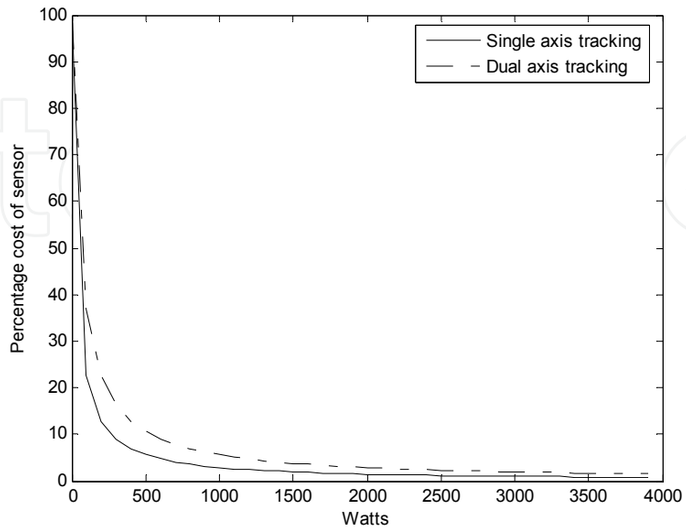

Fig. 1. Percentage sensor cost as a function of installed wattage of photovoltaics

2. The polar-axis photovoltaic solar tracker

The platform carries ten Shott 300W photovoltaic panels. In addition, two smaller, Shell SQ 80W solar panels are provided, to compensate for the energy looses in the electrical installation. The detailed design of the 3KW platform is presented elsewhere (de Lazzer, 2005). The standing 3KW platform is shown in Figure 2. The drive system consists of a d.c motor linked to the platform through a gear train having a gear ratio of 800. Additional provision was made for the occasional manual adjustment of the elevation of the platform for the purposes of field experimentation.

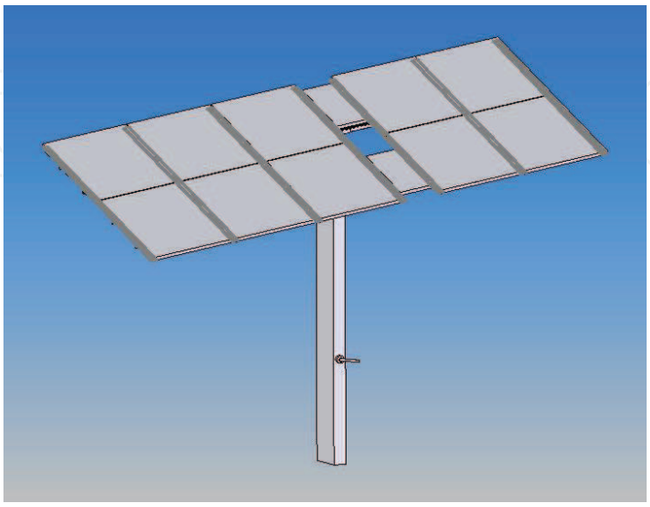

Fig. 2. The 3KW polar-axis solar power platform

2.1 Mathematical modelling of the 3 KW solar power platform

The block diagram representation of the platform in the east-west direction is shown in Figure 3. Where: $\theta_s(t)$ is the instantaneous direction of sunlight and $\theta_p(t)$ the instantaneous position of the platform. Following (de Lazzer, 2005; Agee et al., 2006; Agee & Jimoh, 2007), for the D.C motor we can write:

$$e_a = R_a i_a + L_a \frac{di_a}{dt} + K_b \frac{d\theta_m}{dt} \tag{1}$$

where $e_a(t)$: armature voltage (V); $i_a(t)$: armature current (A); R_a : armature resistance (Ω); L_a : armature inductance (H); K_b : back-emf constant (V/rad/s) and $\theta_m(t)$: rotor displacement (rad.). Similarly, the mechanical torque developed by the motor is given by

$$T_m = K_m i_a \tag{2}$$

where $T_m(t)$ is torque(N.m.) and K_m the torque constant (N.m/A).
Furthermore, the mechanical torque is written as in equation (3).

$$T_m = J_t \frac{d^2\theta_m}{dt^2} + B\frac{d\theta_m}{dt} + K\theta_m \tag{3}$$

where $J_t = J_m + N^2 J_l$ and J_m : moment of inertia of the motor ($kg.m^2$); J_l : moment of inertia of the load($kg.m^2$); N : gear-train ratio between motor and load; B : viscous-friction coefficient of the motor ($kg.m.s^{-1}$); K : spring constant ($kg.m^2.s^{-2}$).
The physical-variables state-space description of the platform, $\dot{x} = Ax + Bu$, could thus be written as:

$$\begin{aligned}
&\dot{x}_1 = x_2 \\
&\dot{x}_2 = -\frac{K}{J_t}x_1 - \frac{B}{J_t}x_2 + \frac{K_m}{J_t}x_3 \\
&\dot{x}_3 = -\frac{K_b}{L_a}x_2 - \frac{R_a}{L_a}x_3 + \frac{1}{L_a}u \\
&y = x_1 = \theta_m ; u = e_a \\
&x^T = [x_1, x_2, x_3] = [\theta_m, \dot{\theta}_m, i_a] \\
&B^T = [0,0,1/L_a]
\end{aligned} \tag{4}$$

3. Differential flatness of platform

By definition, a linear system given by:

$$\begin{aligned}
&\dot{x} = Ax + Bu \\
&x \in R^n, u \in R^m; n \geq m+1
\end{aligned} \tag{5}$$

is said to be differentially flat (or simply *flat*) if it is equipped with a set of variables h_1, called the flat output (Levine & Nguyen, 2003), such that for some integer r,

$$h_1 = g(x, u, \dot{u}, \ddot{u}, ..., u^{(r)}), 0 < r \leq \infty; h_1 \in R^m \tag{6}$$

such that every state $x_i, i = 1, 2, ...n$ of the linear system, together with its input u can be described completely in terms of the flat output and its derivatives as in equation (7).

$$\begin{aligned} x_i &= p_i(h_1, \dot{h}_1, \ddot{h}_1, ..., h_1^{(q)}) \\ u &= Q(h_1, \dot{h}_1, \ddot{h}_1, ..., h_1^{(q+1)}) \end{aligned} \tag{7}$$

Where q is a finite integer, such that the initial equations $\dot{x} = Ap(h_1, \dot{h}_1, \ddot{h}_1, ..., h_1^{(q)}) + BQ(h_1, \dot{h}_1, \ddot{h}_1, ..., h_1^{(q+1)})$, where $\alpha^T = [\alpha_1, \alpha_2, ...\alpha_n]$, are identically satisfied. We shall thus show that every state variable of the physical model of the platform could be written in terms of a set of variables, the flat variable, and a finite number of its derivatives.

3.1 Derivation of the flat output for a linear system with a scalar input

For the given linear system, re-write the dynamics in the formal variable ***s*** as:

$$\begin{aligned} A_1(s)X(s) &= Bu(s) \\ A_1(s) &= sI - A \end{aligned} \tag{8}$$

The formal derivation of the flat output for (8) follows the method of Levine and Nguyen; and requires that there be a matrix C, of rank ***n-m***, orthogonal to ***B*** (Levine & Nguyen, 2003) such that,

$$C^T B = 0 \tag{9}$$

$$C^T A_1(s) P(s) = 0 \tag{10}$$

$$Q(s) = (B^T B)^{-1} B^T A_1(s) P(s) \tag{11}$$

hence, for a given linear system for which $A_1(s)$ and B(s) are known, ***C*** can be evaluated from (9). P(s) is then evaluated from equation (10), and finally, Q(s) is evaluated from equation (11)

3.2 Derivation of the flat output for the polar-axis-type photovoltaic solar power platform

The detailed derivation of the flat output for the polar-axis solar tracker is presented in (Agee & Jimoh, 2010). Key result is summarised as follows:

$$\begin{aligned} p_1(s) &= \frac{K_m}{J_t} h_1(s) \\ p_2(s) &= s p_1(s) \\ p_3(s) &= \left\{ s^2 + \frac{b}{J_t} s + \frac{K}{J_t} \right\} h_1(s) \end{aligned} \tag{12}$$

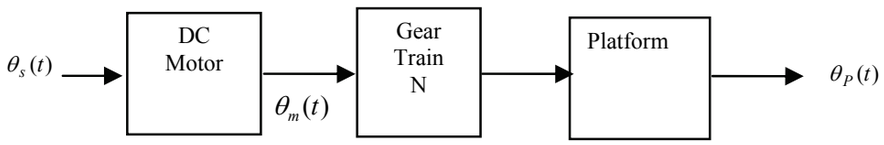

Fig. 3. Block diagram of the open-loop 3KW solar power platform

and $Q(s) = (B^T B)^{-1} B^T A_1(s) P(s)$ yields

$$Q(s) = \left\{ \frac{R_a K}{J_t} + \frac{\{R_a B + K_b K_m + L_a K\}}{J_t} s + \frac{\{L_a B + R_a J\}}{J_t} s^2 + L_a s^3 \right\} h_1(s) \tag{13}$$

It is evident from equation (12) that each of the states of the platform could now be written in terms of the flat output $h_1(t)$ and its derivatives. The input u(t) could be written from equation (13). Hence,

$$\begin{aligned} \theta_m(t) &= \frac{K_m}{J_t} h_1(t) \\ \dot{\theta}_m(t) &= \frac{K_m}{J_t} \dot{h}_1(t) \\ \ddot{\theta}_m(t) &= \frac{K_m}{J_t} \ddot{h}_1(t) \\ i_a(t) &= \ddot{h}_1 + \frac{B}{J_t} \dot{h}_1 + \frac{K}{J_t} h_1(t) \end{aligned} \tag{14}$$

$$\begin{aligned} \theta_p(t) &= \frac{K_m}{800 J_t} h_1(t) \\ \dot{\theta}_P(t) &= \frac{K_m}{800 J_t} \dot{h}_1(t) \end{aligned} \tag{15}$$

$$u(t) = e_a = \frac{R_a K}{J_t} h_1 + \frac{\{R_a B + K_b K_m + L_a K\}}{J_t} \dot{h}_1 + \frac{\{L_a B + R_a J\}}{J_t} \ddot{h}_1 + L_a h_1^{(3)} \tag{16}$$

Alternatively,

$$\begin{aligned} h_1(t) &= \frac{J_t}{K_m} \theta_m(t) \\ \dot{h}_1(t) &= \frac{J_t}{K_m} \dot{\theta}_m(t) \\ \ddot{h}_1 &= i_a(t) - \frac{K}{K_m} \theta_m(t) - \frac{B}{K_m} \dot{\theta}_m(t) \end{aligned} \tag{17}$$

Notice also that, if the desired trajectories of motion are either know apriori, or given, the reference values of the flat output and it derivatives $h_1^*, \dot{h}_1^*, \ddot{h}_1^*, h_1^{(3)*}$, could be described.

3.3 Alternative Description of the Dynamics of the Tracker

The flat description of the systems dynamics, as in equations (14)-(16), enables an alternative

$$\begin{aligned}\dot{h}_1 &= h_2 \\ \dot{h}_2 &= h_3 \\ \dot{h}_3 &= -\frac{R_a K}{J_t L_a} h_1 - \frac{\{R_a B + K_b K_m + L_a K\}}{J_t L_a} h_2 - \frac{\{L_a B + R_a J\}}{J_t L_a} h_3 + \frac{1}{L_a} u(t)\end{aligned} \tag{18}$$

presentation of the dynamics of the platform, in terms of the flat output. Hence, using equation (16), a representation of the plant in terms of the flat output could be presented as in equation (18). The presentation in equation (8) is particularly suitable for controller design.

4. Controller design

The differential flatness property allows to exploit sensor-less control of the platform, in which loop closure is with respect to the time derivation of the angular position of the sun with respect to an earth-based observer. Details are presented in section five of the chapter.

4.1 Controller tuning

For the design of a three-term controller in the flat variables, substitute equation (19) in equation (18),

$$\dot{h}_3(t) = \dot{h}_3^* - K_1(h(t)_1 - h_1^*(t)) - K_2(h_2(t) - h_2^*(t)) - K_3(h_3 - h_3^*(t)) \tag{19}$$

and the steering input is thus given by:

$$\begin{aligned}u_{1c}(t) &= K_1 L_a h_1^*(t) + K_2 L_a h_2^*(t) + K_3 L_a h_3^*(t) + (\beta_1 - K_1) h_1(t) \\ &+ (\beta_2 - K_2 L_a) h_2(t) + (\beta_3 - K_3 L_a) h_3(t) + L_a \dot{h}_3(t)\end{aligned} \tag{20}$$

Where,

$$\beta_1 = \frac{R_a K}{J_t}; \beta_2 = \frac{R_a B + K_b K_m + L_a K}{J_t}; \beta_3 = \frac{L_a B + R_a J}{J_t} \tag{21}$$

the substitution resulting also in the following controlled system in equation (22):

$$\begin{aligned}\dot{h}_1 &= h_2 \\ \dot{h}_2 &= h_3 \\ \dot{h}_3 &= \dot{h}_3^* - K_1 e - K_2 \dot{e} - K_3 \ddot{e} \\ e &= h_1 - h_1^*, \dot{e} - h_2 - h_2^*, \ddot{e} = h_3 - h_3^*, \dddot{e} = \dot{h}_3 - \dot{h}_3^*\end{aligned} \tag{22}$$

with the equivalent characteristics equation given by equation (23).

$$[s^3 + K_3 s^2 + K_2 s + K_1] E(s) = 0 \tag{23}$$

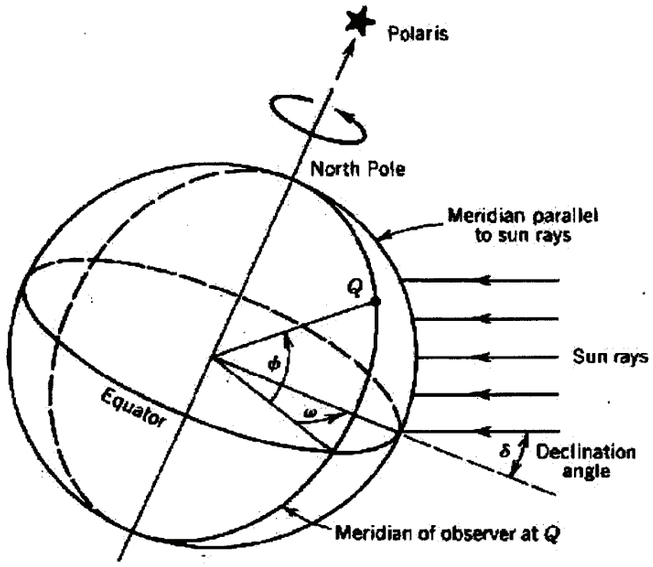

Fig. 4. Measurement of direction of sunrays, in the earth-centred coordinate systems

To obtain the controller parameters K_1, K_2, K_3, the platform is tuned to yield the same dominant pole-pair as in (Agee et al., 2006); with the dominant poles given as $s_1, s_2 = -2.324 + j2.34$ and the third pole given by $s_3 = -33.506$. This system of closed-loop poles leads to the closed-loop dynamics of equations (24) and (25).

$$\begin{aligned} &\dot{h}_1 = h_2 \\ &\dot{h}_2 = h_3 \\ &\dot{h}_3 = -355.7276(h_1 - h_1^*(t)) - 165.0125(h_2 - h_2^*(t)) - 38.114(h_3 - h_3^*(t)) \\ &\therefore K_1 = 335.7276, K_2 = 165.0125, K_3 = 38.114 \end{aligned} \tag{24}$$

$$\begin{aligned} u(t) = u^*(t) + (\frac{R_a K}{J_t} - 355.7276)(h - h^*{}_1) + (\frac{R_a B + K_b K_m + L_a K}{J_t} \\ -165.0125)(h_2 - h_2^*) + (\frac{L_a B + R_a J}{J_t} - 38.114)(h_3 - h_3^*) + L_a \dddot{h}_1 \end{aligned} \tag{25}$$

In equation (25), it has also been assumed that the reference acceleration $\dot{h}_3^*(t) = 0$, for bravity.

4.2 Classical control of polar-axis tracker with a solar position sensor

In the classical control of systems, feedback loop closure is with respect to the expected steady-state values of state. Suppose that the tracker is at rest at an initial position $\theta_p(0)$; for generality, use the notation

$$\theta_p(0) = 0 \tag{26}$$

Also at this rest position, all velocities and accelerations are zero. Hence, $\dot{\theta}_P(0) = \ddot{\theta}_P(0) = 0....$ It also follows from equations (14)-(17) that:

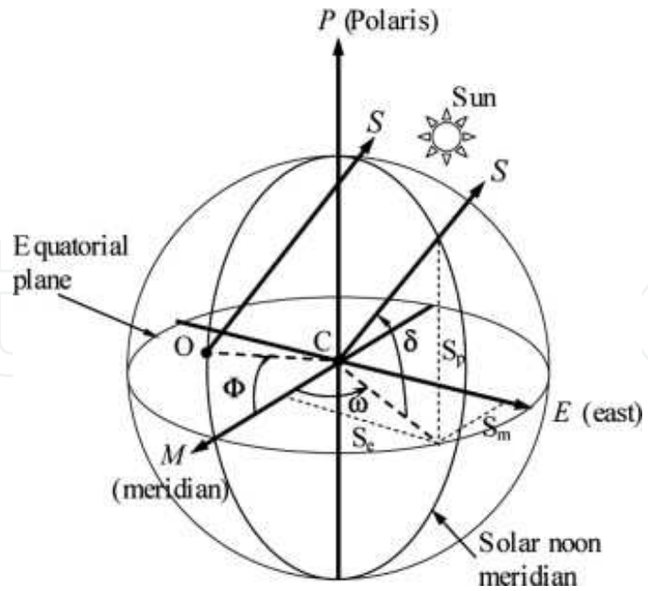

Fig. 5. Relationship between earth-centred solar coordinates and the perpendicular coordinates used on the surface of the earth

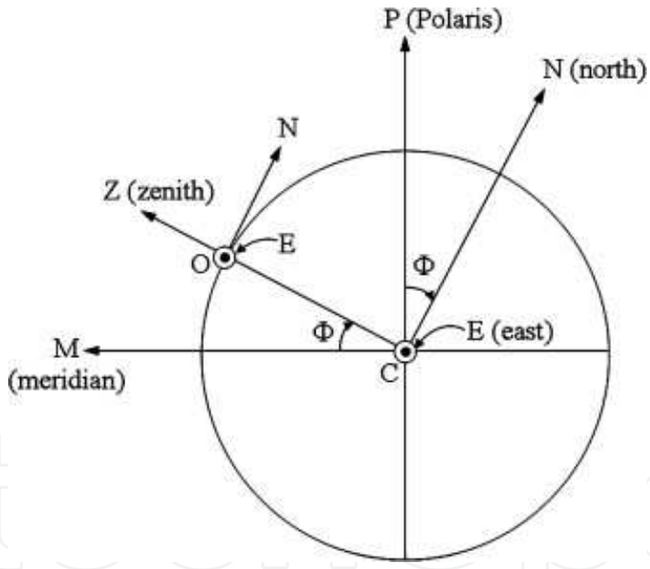

Fig. 6. Reference from equatorial plane to the plane of observer latitude

$$\theta_m(0) = h_1(0) = 0$$
$$\dot{\theta}_m(0) = \dot{h}_1(0) = \ddot{\theta}_m(0) = \ddot{h}_1(0) = 0 \tag{27}$$

And the classical control strategy is implemented as in equation (29):
Suppose that the sensor updates its output to a non-zero step change in the direction of sunrays $\dot{\theta}_P(t)$. The tracker will respond and track this new direction, which becomes the desired steady state direction of the sunrays; or $\dot{\theta}_P(t) = \theta_P(\infty)$, then for the new angular position of the sun:

$$h_1^*(t) = h_1(\infty) = \frac{800J_t}{K_m}\theta_P(\infty), h_2^*(t) = \dot{h_2}(\infty) = 0, h_3^*(t) = h_3(\infty) = 0 \tag{28}$$

$$\begin{aligned}
\dot{h_1} &= h_2 \\
\dot{h_2} &= h_3 \\
\dot{h_3} &= -355.7276(h_1 - h_1^*(\infty)) - 165.0125h_2 - 38.114h_3 \\
u(t) &= (\frac{R_aK}{J_t} - 355.7276)\{\ h_1(t) - \frac{800J_t}{K_m}\theta_P(\infty)\ \} \\
&\quad + (\frac{R_aB + K_bK_m + L_aK}{J_t} - 165.0125)h_2 + (\frac{L_aB + R_aJ}{J_t} - 38.114)h_3
\end{aligned} \tag{29}$$

4.3 Design of controller with trajectories of sunrays

The flatness property enables to integrate the mathematical formula for the trajectory of sunrays into the controller structure. These trajectories are derived in the sequel.

5. Derivation of the direction of sun rays as a function of local clock time

Sensorless solar tracking has been applied in solar-thermal systems (Ibrahim et al., 2004; Cheng & Wong, 2009; Power from the Sun, 2010; Chen et al., 2006; Stine & Harrington, 1988), and uses the concept of solar time and solar angle to relate the time of the day and time of the year to the position of the sun. For the derivation of the mathematical relationships employed in sensor-less solar tracking, consider first Figure 4, which shows the traditional measurement of the direction of sunrays, in a coordinate system with its origin as the centre of the earth. This coordinate system has one axis pointing toward the poles of the earth, and the other being the equatorial plane of the earth. Consider also the sunrays having an instantaneous declination δ with respect to the equatorial plane, through a meridian that differ from the meridian ***O***, of the observer (the observer here being the polar-axis solar platform) by an angle (the solar angle) ω. The solar angle being the difference between the current meridian (or longitude) of sunrays and the observer meridian.

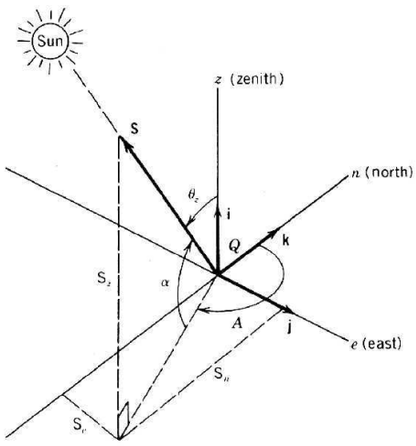

Fig. 7. Collector-centred coordinate systems and its realtionship to the earth-centred co-ordinates at the observer location

On the earth surface however, an observer uses a set of co-ordinates wherein, one of the cardinal axes points vertically upward, and the remaining two point north-south and east-west respectively. Figure 5 shows the relative orientations of the original solar co-ordinates and those used by an observer at the surface of the earth. The directional cosines relating the two co-ordinate systems [S], at the equator, are given by (Ibrahim et al., 2004; Cheng & Wong, 2009; Power from the Sun, 2010; Chen et al., 2006; Stine & Harrington, 1988) as:

$$[S] = \begin{bmatrix} S_m \\ S_e \\ S_p \end{bmatrix} = \begin{bmatrix} \cos\delta\cos\omega \\ -\cos\delta\sin\omega \\ \sin\delta \end{bmatrix} \tag{30}$$

Referred to the observer latitude Φ at position ***O***, as shown in Figure 6, a further set of angular transformations is given by equation (31):

$$\left[\Phi\right] = \begin{bmatrix} \cos\Phi & 0 & \sin\Phi \\ 0 & 1 & 0 \\ -\sin\Phi & 0 & \cos\Phi \end{bmatrix} \tag{31}$$

where is Φ the latitude angle.

For a tracking collector mounted on a stand, motion is only possible in two axes. Hence, for the collector surface located at ***O***, the solar position is measured in terms of an observer-centred cordinate system, consisting of a vertical (OV) or zenith (OZ) axis, and a horizontal (OH) axis. The elavation angle α (or its complement, the zenth angle θ_Z) and the azimuth angle β are therefore sufficient descriptors of the colloctor orientation in the OV-OH plane. This collector-centred co-ordinate system compares with the earth-surface co-ordinates as shown in Figure 7. The collector orientation is shown in Figure 8, and the orientation admits the representation in equation (32):

$$S^{/} = \begin{bmatrix} S_V \\ S_H \\ S_R \end{bmatrix} = \begin{bmatrix} \sin\alpha \\ \cos\alpha\sin\beta \\ \cos\alpha\cos\beta \end{bmatrix} \tag{32}$$

The collector elavation α, and its azimuth β, are the required tracking angles. In an ideal azimuth-elavation system, OV, OH and OR axes of the collector-centred frame are parallel to the OZ, OE and ON axes of the earth-surface frame, as shown in Figure 9. Generally, this coincidence may not apply, and the two co-ordinates are rotated from each other. The three possible scenarios are as illustrated in Figure 10. The associated transformation angles of the three orientations are given by equations (33)-(35):

$$\left[\varphi\right] = \begin{bmatrix} 1 & 0 & 0 \\ 0 & \cos\phi & -\sin\phi \\ 0 & \sin\phi & \cos\phi \end{bmatrix} \tag{33}$$

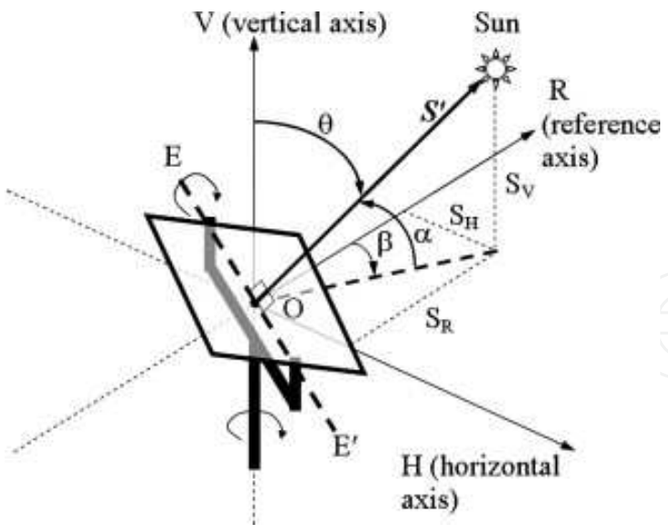

Fig. 8. Orientation of the collector in the OV-OH-OR axes

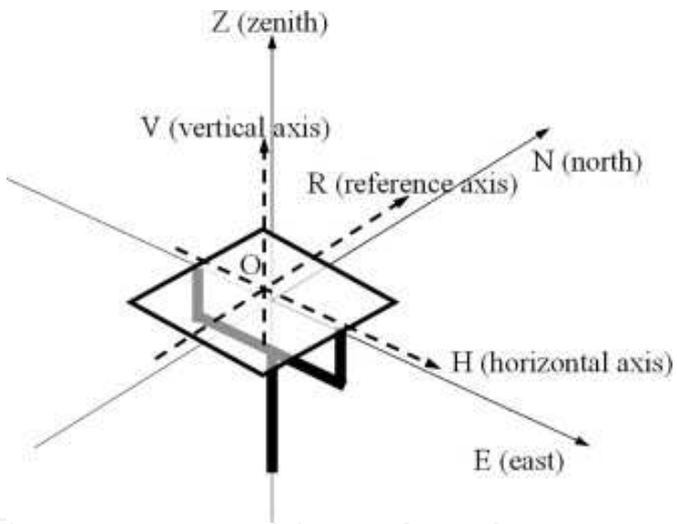

Fig. 9. Ideal orientation of collector in the OV-OH-OR axes

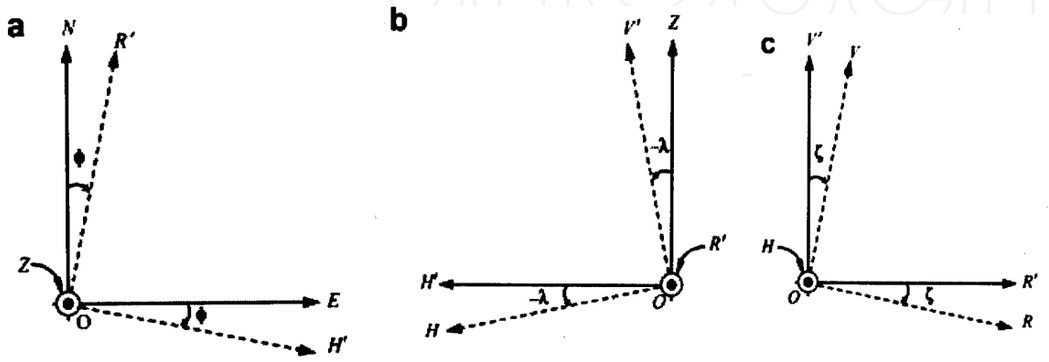

Fig. 10. Orientations of the OV-OH-OR axes relative to the OZ-OE-ON axes

$$[\lambda]=\begin{bmatrix}\cos\lambda & -\sin\lambda & 0\\ \sin\lambda & \cos\lambda & 0\\ 0 & 0 & 1\end{bmatrix} \tag{34}$$

$$[\zeta]=\begin{bmatrix}\cos\zeta & 0 & \sin\zeta\\ 0 & 1 & 0\\ -\sin\zeta & 0 & \cos\zeta\end{bmatrix} \tag{35}$$

The overall cosine angles are threfore given by the combined transformation as in equation (36):

$$\begin{bmatrix}S_V\\ S_H\\ S_R\end{bmatrix}=\begin{bmatrix}\sin\alpha\\ \cos\alpha\sin\beta\\ \cos\alpha\cos\beta\end{bmatrix}=[\zeta][\lambda][\phi][\Phi]\begin{bmatrix}\cos\delta\cos\omega\\ -\cos\delta\sin\omega\\ \sin\delta\end{bmatrix} \tag{36}$$

Solving the above matrix equation for the solar altitude angle in the collector-centred frame, we have for α, the elavation angle of the sun with respect to the orientation of the platform, given by:

$$\begin{aligned}&\alpha=\sin^{-1}\{ab+c+d\}\\ &a=\cos\delta\cos\omega\\ &b=\cos\zeta\cos\lambda\cos\Phi-\cos\zeta\sin\lambda\sin\phi\sin\Phi-\sin\zeta\cos\phi\sin\Phi\\ &c=-\cos\delta\sin\omega[\sin\zeta\sin\phi-\cos\zeta\sin\lambda\cos\phi]\\ &d=\sin\delta[\cos\zeta\cos\lambda\sin\Phi+\cos\zeta\sin\lambda\sin\phi\cos\Phi+\sin\zeta\cos\phi\cos\Phi]\end{aligned} \tag{37}$$

Or the zenith angle

$$\theta_Z=\frac{\pi}{2}-\alpha \tag{38}$$

Similarly, the azimuth angle is given by:

$$\begin{aligned}&\beta=\begin{cases}\sin^{-1}\left\{\dfrac{ae+m+f)}{\cos\alpha}\right\};\beta\geq 0\\ \pi-\sin^{-1}\left\{\dfrac{ae+m+f)}{\cos\alpha}\right\};\beta<0\end{cases}\\ &a=\cos\delta\cos\omega\\ &e=\sin\lambda\cos\Phi+\cos\lambda\sin\phi\sin\Phi\\ &m=-\cos\delta\sin\omega\cos\lambda\cos\phi\\ &f=\sin\delta[\sin\lambda\sin\Phi-\cos\lambda\sin\phi\cos\Phi]\end{aligned} \tag{39}$$

and because β can exist in any of the four quadrants, depending on the observer location on the earth, time of the day and season of the year, the following two evaluations must be jointly made to determine the quadrant of β, hence its actual value.

$$\begin{aligned}
&\sin\beta = \frac{g+h+i}{\cos\alpha} \\
&g = \cos\delta\cos\omega[\sin\lambda\cos\Phi + \cos\lambda\sin\phi\sin\Phi] \\
&h = -\cos\delta\sin\omega\cos\lambda\cos\phi \\
&i = \sin\delta[\sin\lambda\sin\Phi - \cos\lambda\sin\phi\cos\Phi]
\end{aligned} \tag{40}$$

$$\begin{aligned}
&\cos\beta = \frac{aj+k+l}{\cos\alpha} \\
&a = \cos\delta\cos\omega \\
&j = -\sin\zeta\cos\lambda\cos\Phi + \sin\zeta\sin\lambda\sin\phi\sin\Phi - \cos\zeta\cos\phi\sin\Phi \\
&k = -\cos\delta\sin\omega[\sin\zeta\sin\lambda\cos\phi + \cos\zeta\sin\phi] \\
&l = \sin\delta[-\sin\zeta\cos\lambda\sin\Phi - \sin\zeta\sin\lambda\sin\phi\cos\Phi + \cos\zeta\cos\phi\cos\Phi]
\end{aligned} \tag{41}$$

5.1 Special cases of observer solar angles

Special cases of the sun angles from the collector are presented by (Ibrahim et al., 2004). For example, for elavation-azimuth tracking, set the angles $\phi = \pi$, $\lambda = 0$ and $\zeta = \Phi - \pi/2$ in the general formulas. For this case, the general tracking formula can be then simplified to

$$\begin{aligned}
&\theta_Z = \pi/2 - \delta \\
&\beta = \omega
\end{aligned} \tag{42}$$

Where θ_Z is the zenith angle, and β is the azimuth angle. In polar-axis tracking, the zenith angle is fixed (or seassonally fixed), as a function of the local lattitude angle. The azimuth anlge information is then available for one-axis tracking, from sunrise to sunset. From equation (42), the azimuth angle at any instant of time has the value of the sun hour angle, ω. Now, from (Power from the Sun, 2010),

$$\beta = \omega = 15(t_s - 12)^o; -180^o \le \omega \le 180^o \tag{43}$$

and t_s the solar hour, ω the solar angle is zero degrees when the sun is directly overhead, or when the solar hour is 12.00hrs.

5.2 Relating the azimuth angle of sunrays to the local clock time

The solar hour may differ from the local clock time (LCT). This difference is quantified by the equation-of-time (EOT). A version of the EOT which is accurate to within 0.63 seconds is given by (Power from the Sun, 2010):

$$EOT = \sum_{K=0}^{5}\left\{A_K\cos\left(\frac{360Kn}{365.25}\right) + B_K\sin\left(\frac{360Kn}{365.25}\right)\right\}[hours] \tag{44}$$

Where the A_K's and B_K's are given in Table 1 and ***n*** is the number of days into a leap year cycle, with ***n=1*** being January of each leap year and ***n=1461*** corresponding to 31st December of the 4th year in a leap year cycle. The complete relationship between solar time and the local clock time is given in equation (45):

$$t_s = LCL + EOT - LC - D[hours] \tag{45}$$

K	A_K(hr)	B_K(hr)
0	2.0870×10^{-4}	0
1	9.2869×10^{-3}	-1.2229×10^{-1}
1	-5.2258×10^{-2}	-1.5698×10^{-1}
3	-1.3077×10^{-3}	-5.1602×10^{-3}
4	-2.1867×10^{-3}	-2.9823×10^{-3}
5	-1.5100×10^{-4}	-2.3463×10^{-4}

Table 1. Coefficients for conversion between solar time and clock time

D is 1 hour where daylight saving time is used, otherwise, D=0. In South Africa, D=0. The local longitude correction (LC) is given by:

$$LC = \frac{LL - LoLTz}{15}[hours] \tag{46}$$

where ***LC*** : the longitude collection, ***LL*** : local logitude at the location of the local time clock, and ***LoLTz*** : Longitude of the standard time zone meridian. Summarising equations (43-46), the azimuth direction of sunrays, at a given location, as a function of time in seconds could be re-written as in equation (47).

$$\begin{aligned} &\beta_s(t) = \frac{15}{3600}t - 180 \quad [\deg rees] \\ &0 \le t \le 86400\sec \end{aligned} \tag{47}$$

And local clock time in seconds have been used in equation (47), instead of LCT. Given that no tracking is needed before sunrise, and after sunset, equation (47), may be written as

$$\begin{aligned} &\beta_s(t) = 0.00416667(t - t_R) + \beta_R(0) - 180 \quad [\deg rees] \\ &t_R \le t \le t_S \end{aligned} \tag{48}$$

Where t_R is the sunrise time (seconds) at the location, $\beta_R(0)$=0.004166 t_R is the sunrise angle, and t_s is the sunset time.

5.3 Trajectories generation for sensorless tracking

To generate trajectories of motion for sensorless control, substitute equation (48) into equation (17) to obtain equation (49), for which the reference trajectories for feedback are given by:

$$\begin{aligned} h_1^*(t) &= \frac{K_m}{J_t}\beta_s(t) \\ h_2^*(t) &= \frac{K_m}{J_t}\dot{\beta}_s(t) \\ h_3^*(t) &= \frac{K_m}{J_t}\ddot{\beta}_s(t) \end{aligned} \tag{49}$$

Which, by substitution yields:

$$h_1^*(t) = 0.00416667\frac{K_m}{J_t}t; h_1^*(0) = 0.00416667\frac{K_m}{J_t}t_R$$
$$h_2^*(t) = 0.00416667\frac{K_m}{J_t}; h_2^*(0) = 0 \quad (50)$$
$$h_3^*(t) = 0, h_3^*(0) = 0$$

6. Simulations, results presentation and discussion

Simulation results present the dynamic response of the open-loop platform, the impact of feedback on platform performance, and the performance of the platform in tracking the direction of sunrays through sensorless control.

6.1 System data

The data used for the simulation of the platform systems is shown in Table 2.

R_a=5Ω	L_a=0.003H	B=3.95.10^{-6} Kg.ms^{-1}
K_b=0.0636V/rad/s	K_m=0.00711 Kgm/A	K=0.01Kgm^{2}s^{-2}
J_M=7.72.10^{-6} Kg m^2	J_L=970Kgm^2	N=1/n=1/800

Table 2. Platform system parameters

6.2 Dynamics of uncontrolled platform

The dynamics of the uncontrolled platform is shown in Figure 11. Overshoots of 96% are confirmed in the rotor position and speed. The settling time is 102seconds. The results confirm those presented in (de Lazzer, 2005; Agee et al., 2006).

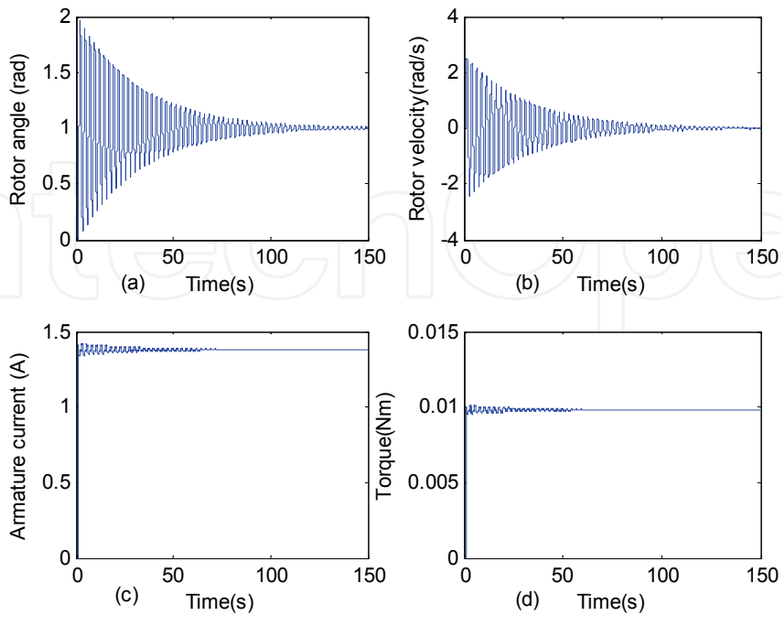

Fig. 11. Dynamics of open-loop platform

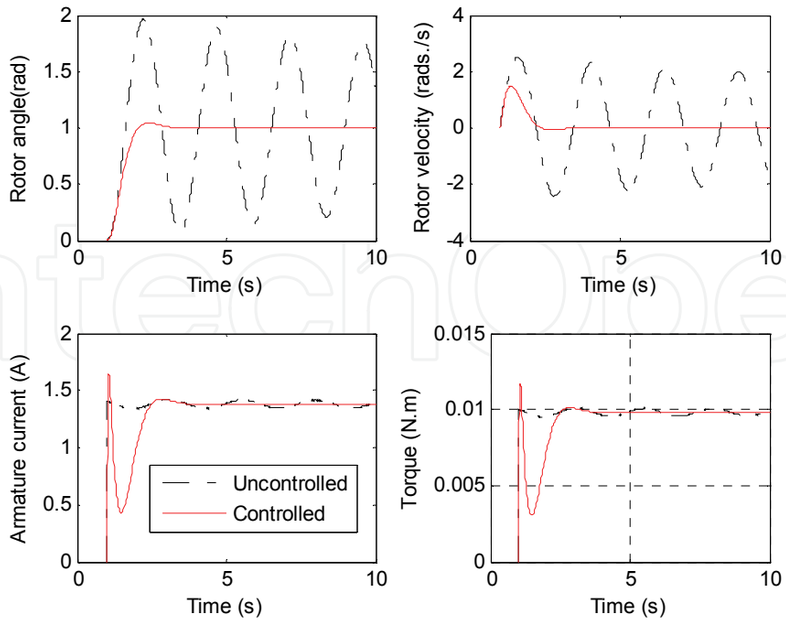

Fig. 12. Comparison of dynamics for controlled and uncontrolled platform

6.3 Dynamics of platform controlled by classical three-term controller

The effect of including a classical linear three-term controller is shown in Figure 12. Compared to the dynamics of the uncontrolled platform, the controller brings the systems to settle in about 2 seconds. Overshoots of the rotor angle and velocity are within the acceptable limit of 17% (Kuo and Galnoraghi, 2003). However, the overshoots in the motor armature current and the delivered torque have been worsened by the inclusion of the classical controller. Current overshoots and torque overshoots have implications in the choice of the rating and costs of the drive systems, as well as the extra installed PV capacity required for the drive hardware.

6.4 Performance of controlled platform with trajectories of motion

Figures 13-15 show the dynamics of the platform in sensorless tracking. In Figure 13, we see that the tracking of the direction of the sunrays is achieved within a second, and without oscillations. From Figures 14 and 15, we could conclude that the transient velocity (maximum value of about 0.003.8deg./sec) and maximum acceleration (0.02deg./sec^2) were not excessive. As such, the energy required for sensorless tracking is low. This is a major factor of merit when considering also the cost of supplying the tracker drive system.

7. Conclusions

In conclusion, a flat model of the solar tracker was presented and used for controller design. Mathematical derivation of the direction of sunrays as a function of the local clock time was given. It was also shown how the flatness property could be combined with the mathematical formulation of the direction of sunrays to generate trajectories of motion for sensorless tracking. Results also showed that sensorless tracking was achieved without oscillations, at modest velocities and accelerations. The low energy requirement in

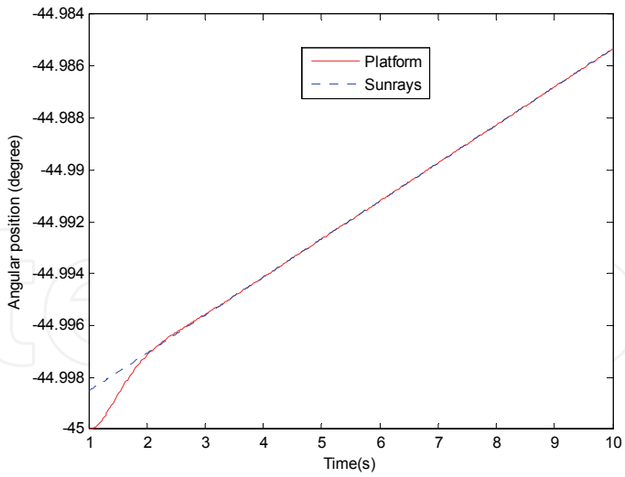

Fig. 13. Polar axis tracking of angle of sunrays

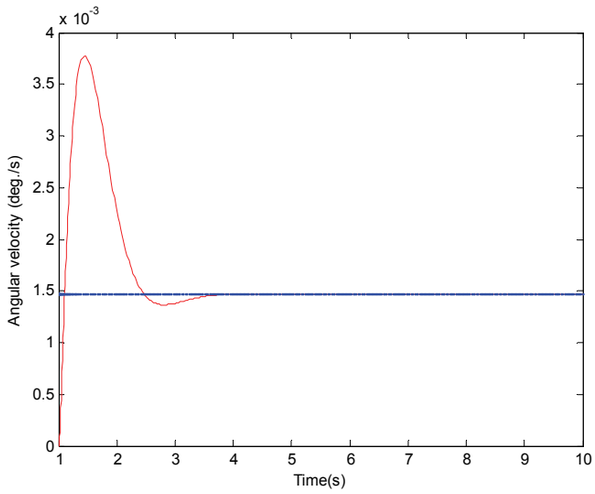

Fig. 14. Velocity response of tracker

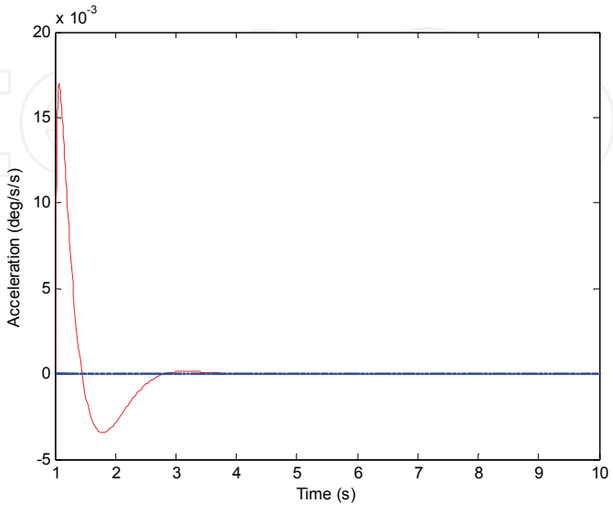

Fig. 15. Comparison of acceleration

sensorless tracking could be beneficial in reducing the rating requirements of auxiliary photovoltaic power, required for the tracker drive system. Combined with the elimination of sensor cost, the reduced drive energy requirement could lead to significant reductions in the overall cost of photovoltaic hardware.

8. References

Agee, J. T. Obok-Opok, A. and de Lazzer, M. (2006). "Solar tracker technologies: market trends and field applications. *Int. Conf. on Eng. Research and Development: Impact on Industries*. 5-7th September, 2006.

Agee, J. T. , de Lazzer, M. an Yanev, M. K. "A Pole cancellation strategy for stabilising a 3KW solar power platform. *Int. Conf. Power and Energy Systems(EuroPES 2006*), Rhodes, Greece. June 26-28.

Agee, J. T. and Jimoh, A. A. (2010) Flat Control of a Polar-Axis Photovoltaic Solar power Platform. Submitted.

Greenology (2010). Available on http://www.greeology.co.za, 25th June, 2010

Bitaud, L., Fliess, M. and Levine, J. (2003).A Flatness-Based Control Synthesis of Linear Systems and Application to Wind Sheild Wiper. Proceedings of the European Control Conference (ECC'97), Brussels. Pp. 1-6.

Cheng, K. K. and Wong, C. W. (2009). General Formula for Ones-axis Tracking Systems and its Application in Improving Tracking Accuracy of Solar Collectors. Solar Energy vol. 83, Issue 3, pp. 298-305.

Chen, Y. T., Lim, B. H. and Lim, C. S (2006). General Sun Tracking Formula for Heliostats with Arbitrary Oriented Axes, Journal of Solar Energy, vol 128, pp. 245-250.

De Lazzer, M. *Positioning System for an Array of Solar Panels (*M.Eng Thesis (Unpublished). University of Botswana and Ecoles de Saint Cyr, France, 2005).

Energy from the Desert (2003): Practical Proposals for Large Scale Photovoltaic Systems. Edited bt: Kusoke Korokawa, Keiichi Komoto, Peter van der Vlueten and David Faiman. Pp. 150.

Fliess, M., Levine, J, Martan, P., Ollivier, F. and Rouchon, P. (1997).Controlling Nonlinear Systems by Flatness. In Systems and Control in the Twenty-first Century (Progress in Systems and Control Theory); ed. Byrness, C. I., Datta, B. N., Gilliam, S. And Martin, C. F. Birhauser, Boston. Pp. 137-154.

Fliess, M, Levine, J, Martin, P and Rouchon, P. (1990). A Lie-Backland Approach to Equivalence and Flatness of Nonlinear Systems. IEEE Transactions in Automatic Control; vol. 44, no.5, pp. 922-937.

Kuo, B. C. and Golnaraghi, F. *Automatic Control Systems* (eight edition, John Wiley and Sons, Inc., 2003).

Stine, W. B. And Harringan, R. W. (1985) Solar Energy Fundamentals and design (First ed.). Willey Interscience, New York. Pp. 38-69.

The Suns position. Available on http://www.powerfromthesun.net/chapter3/chapter3word.htm, 25th June, 2010

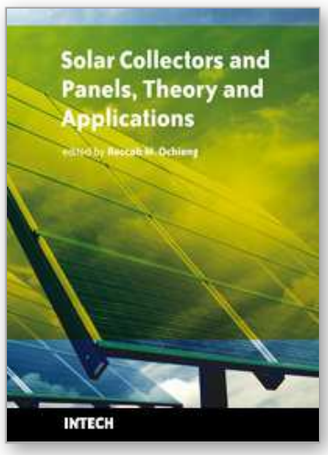

Solar Collectors and Panels, Theory and Applications

Edited by Dr. Reccab Manyala

ISBN 978-953-307-142-8
Hard cover, 444 pages
Publisher Sciyo
Published online 05, October, 2010
Published in print edition October, 2010

This book provides a quick read for experts, researchers as well as novices in the field of solar collectors and panels research, technology, applications, theory and trends in research. It covers the use of solar panels applications in detail, ranging from lighting to use in solar vehicles.

How to reference

In order to correctly reference this scholarly work, feel free to copy and paste the following:

John Agee (2010). Sensorless Controll of a PVC Platform, Solar Collectors and Panels, Theory and Applications, Dr. Reccab Manyala (Ed.), ISBN: 978-953-307-142-8, InTech, Available from: http://www.intechopen.com/books/solar-collectors-and-panels--theory-and-applications/sensorless-control-of-a-pvc-platform

INTECH
open science | open minds

InTech Europe
University Campus STeP Ri
Slavka Krautzeka 83/A
51000 Rijeka, Croatia
Phone: +385 (51) 770 447
Fax: +385 (51) 686 166
www.intechopen.com

InTech China
Unit 405, Office Block, Hotel Equatorial Shanghai
No.65, Yan An Road (West), Shanghai, 200040, China
中国上海市延安西路65号上海国际贵都大饭店办公楼405单元
Phone: +86-21-62489820
Fax: +86-21-62489821

IntechOpen